Lab on a Chip

Cite this: DOI: 10.1039/c2lc20994b

www.rsc.org/loc

PAPER

Concentration landscape generators for shear free dynamic chemical stimulation†

Mathieu Morel,[a] Jean-Christophe Galas,[ab] Maxime Dahan*[a] and Vincent Studer*[cd]

Received 14th October 2011, Accepted 10th January 2012
DOI: 10.1039/c2lc20994b

In this paper we first introduce a novel fabrication process, which allows for easy integration of thin track-etched nanoporous membranes, within 2D or 3D microchannel networks. In these networks, soluble chemical compounds can diffuse out of the channels through well-defined and spatially organized microfabricated porous openings. Interestingly, multiple micron-scale porous areas can be integrated in the same device and each of these areas can be connected to a different microfluidic channel and reservoir. We then present and characterize several membrane-based microdevices and their use for the generation of stable diffusible concentration gradients and complex dynamic chemical landscapes under shear free conditions. We also demonstrate how a simple flow-focusing geometry can be used to generate "on-demand" concentration profiles. In turn, these devices should provide an ideal experimental framework for high throughput cell-based assays: long term high-resolution video microscopy experiments can be performed, under multiple spatially and temporally controlled chemical conditions, with simple protocols and in a cell-friendly environment.

Introduction

In the past few years, there has been a growing interest in micropatterning techniques and microfluidic devices enabling the generation of precise and complex concentration maps of bound and diffusible molecules. These microdevices open the way to concentration-dependent and combinatorial studies for chemical synthesis, biochemistry and biology. In the case of cell biology, microfluidics has shown a great promise in recreating/mimicking gradients of diffusible molecular cues occurring *in vivo*. The spatial and temporal tuning of the stimulation, coupled to the possibility of imaging single cells with high resolution, shall contribute to unraveling fundamental mechanisms of gradients sensing, polarization, migration or differentiation taking place in living organisms.

Since the early 2000's, many groups have developed devices taking advantage of the laminarity and mass transfer phenomena in microflows to measure the response of cells, placed in a channel, to tailored chemical stimulations.[1–3] However with adherent cells, the presence of continuous flows inevitably leads to shear stress on the cell membrane. This mechanical stress has several, potentially detrimental, side effects. For instance, it may affect cellular morphology, trigger cellular signals that can interfere with the basal or chemotactic response,[4,5] induce cell differentiation,[6] or in more extreme cases—*e.g.* neurons—lead to cell death. In addition, cells are susceptible to modify locally the flow pattern and, thereby, the predicted concentration profile.[7]

Several attempts have been made to meet the challenge of gradient generation in a low- or no-flow microenvironment.[8] Two main approaches can be considered. The first is based on the local decrease of hydrodynamic resistance—*e.g.* with micro-grooves for cell culture.[9] In contrast, the second approach consists in a local and drastic increase of the hydrodynamic resistance at the interface between cell culture chambers and stimulation channels. This latter solution is illustrated by ladder devices where cells are cultured in chambers connected with small openings to stimulation channels,[3,10,11] or by devices made of permeable hydrogels where flowing solutes diffuse to the cell chamber through channel borders.[12,13] The generation of the concentration gradient relies on free diffusion between a source and a sink channel that are constantly replenished. Such devices have the advantage of generating a stable steady-state gradient and maintaining the natural cellular environment.[14] Nevertheless the position of the source and sink channels, determined by the microfabrication, limits the concentration profiles that could be obtained and the fixed geometry prevents any dynamic adjustment of the profile during experiments. Moreover, establishment of the gradient is based on the cue diffusion over a large distance

[a]*Laboratoire Kastler Brossel, CNRS UMR8552, Département de Physique et Institut de Biologie, Ecole Normale Supérieure, Université Pierre et Marie Curie – Paris 6, 46 rue d'Ulm, 75005 Paris, France. E-mail: maxime.dahan@lkb.ens.fr*
[b]*Laboratoire de Photonique et de Nanostructures, CNRS UPR20, Marcoussis, France*
[c]*Univ. Bordeaux, Interdisciplinary Institute for Neuroscience, UMR 5297, F-33000 Bordeaux, France*
[d]*CNRS, Interdisciplinary Institute for Neuroscience, UMR 5297, F-33000 Bordeaux, France. E-mail: vincent.studer@u-bordeaux2.fr*

† Electronic supplementary information (ESI) available: A video showing the rotating gradient (M1), and supplementary protocols for micro-well fabrication and cell culture. See DOI: 10.1039/c2lc20994b

(hundreds of microns to millimetres) or through highly viscous materials. This results in a decrease of the temporal resolution of the stimulation, although some devices have been proposed to fasten the gradient installation.[15–17]

A strategy to overcome these drawbacks is to overlay a layer of high-flow rate channels on top of a layer of low-flow cell culture chambers. To this aim, some groups have developed microdevices that integrate semi-porous membranes, at the interface between the two layers, which block the flow in the cell channel.[18–21] This solution is potentially advantageous and flexible as it reduces the diffusing distance between microflows and cells, while allowing the generation of complex and dynamic concentration profiles in the high-flow channel. However, such devices have so far required complex fabrication methods for the membrane sealing, particularly due to the low adhesion of PDMS without surface treatment, often leading to leakage or membrane detachment.[22] The firm attachment of the membrane is mainly done by the superposition of the upper and lower layers. Furthermore, plating cells in these multilayer systems often requires a delicate adjustment of culture protocols, which make them impractical for the study of delicate cultured cells, such as neurons or stem cells.

Here, we propose to modify a fabrication process of photocurable resin-based microdevices ("microfluidic stickers")[23,24] to form membrane openings at the surface of microchannels (Fig. 1). With this technology, we obtain a single layer of channels embedding membranes of different compositions and pore diameters without any leakage. These devices can then be reversibly attached to another layer of open wells in which cells have been plated beforehand, using double-sided tape or magnets (Fig. 2). This architecture allows us to generate and tune diffusive gradients of various concentration profiles—possibly of complex shapes—without shear stress on cells during experiments. By decoupling the cell culture environment from the microfluidic stimulation,[24,25] our devices greatly simplify experiments on biological samples requiring long growth times, such as cultured neurons[26] (Fig. 2D), or which are difficult to position in a closed microenvironment, such as explants or tissues. They also provide an interesting screening platform for cell-based assays with ultrasensitive fluorescence measurements down to the single molecule resolution.

In this article, we first present the principle of our microdevice and its fabrication method. We next characterize the dynamics and stability of simple concentration profiles by combining fluorescence measurements and a numerical diffusion model. Different devices are then proposed in order to generate simple gradients and address issues of spatial dynamics, long-term stability and low sample consumption using multiple membrane openings connected to independent microchannels. We also present devices with patterned porous openings to generate complex and dynamic chemical landscapes. Finally we show how

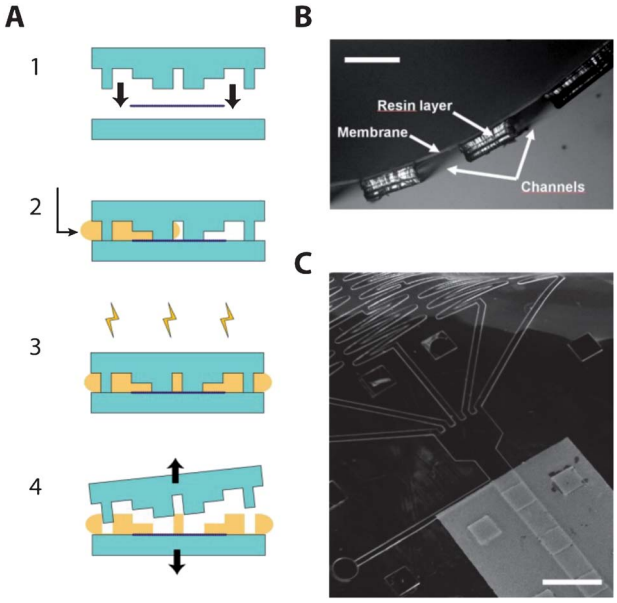

Fig. 1 Fabrication process of the membrane-containing resin layer. (A): (1) A piece of porous membrane is pinched between flat and two-level PDMS molds. (2) This sandwich is then filled with the liquid glue NOA 81 by capillarity. PDMS studs designed in the two-level mold prevent locally the filling of the membrane. (3) Once the assembly is completely filled the resin is cured by UV exposure. (4) The stiff layer of resin embedding the membrane can finally be detached from PDMS molds. (B) Transverse view of a structured layer of resin embedding a membrane. Scale bar 250 μm. (C) Top view of the layer structured with a gradient generator network and embedding a 5 × 10 mm² membrane. The protection of 1 × 1 mm² squares by the PDMS mold forms porous openings in the central microchannel after curing. Scale bar 2.5 mm.

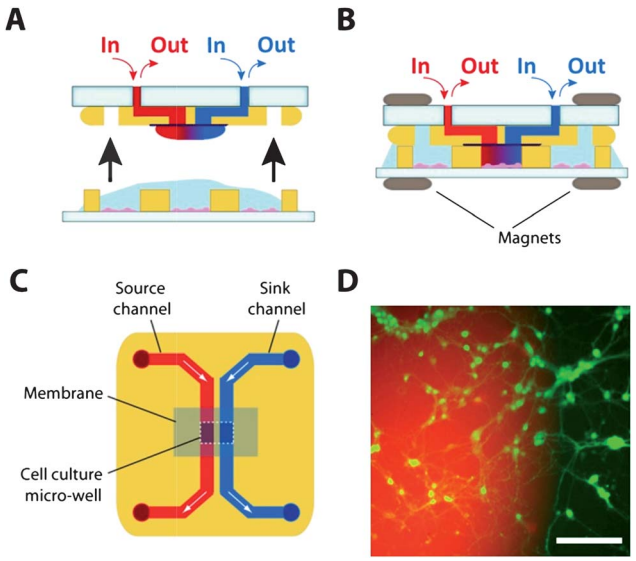

Fig. 2 Use of the membrane-based microdevice for cell-based assays. (A) Transverse view. The microsystem consists of two parts: (i) a structured layer of resin closed by a glass slide with drilled holes and embedding a porous membrane and (ii) a coverslip patterned with open micro-wells for cell culture. (B) The two parts are then reversibly sealed using magnets. The gradient is confined in the micro-wells and remains stable during time. (C) Top view of a simple circuit geometry with two independent channels. Here, a single cell culture chamber is connected to a source and a sink diffusing ports. (D) Cells are grown in the micro-wells with regular protocols. Before experiments, they are placed in front of the membrane openings and the stimulating solute is flowed in the upper microchannel. Here, in green, a primary culture of rat spinal cord neurons is cultured 5 days *in vitro* and submitted to a rhodamine-labeled dextran 70 M_w gradient (in red). Scale bar 100 μm.

the combination of our membrane-based systems with a classical flow-focusing device enables the generation of arbitrarily complex spatio-temporal shear-free concentration patterns.

Results and discussion

Device design and microfabrication

Since PDMS is characterized by its low adhesion to other polymers, we used UV curable glues known for their sticky properties after partial curing.[23,24] Taking advantage of the moderate viscosity of these glues (mainly NOA 81, Norland Products Inc, NJ), we could fully integrate pieces of commercial membranes inside a single layer of this material, by inserting the glue inside a closed mold embedding the membrane. The fabrication protocol is as follows. First, a two-level PDMS stamp was made by conventional PDMS replica molding of a photolithographed 60/120 μm SU-8 mold (MicroChem, MA).[27]

The surface of this replica was then passivated with a perfluorosilane (Sigma Aldrich, France), and the PDMS invert replica was made by conventional molding. A piece of commercial membrane (*e.g.* Cyclopore, ~20 μm thickness, 400 nm hole diameter, Whatman, NJ) was aligned and pressed between this two-level PDMS stamp and a PDMS flat layer (Fig. 1, A1). The space in between was then capillary-filled with liquid NOA 81 (Fig. 1, A2). The PDMS studs in contact with the membrane prevented locally the filling by resin. Less than 250 μL of resin are sufficient to form a 25 × 50 mm^2 layer. Once the filling was complete, a uniform 365 nm illumination (LC8 lamp, Hamamatsu Photonics, France) for 15 s at 10 mW cm^{-2} through the PDMS was performed (Fig. 1, A3).

A stiff micro-patterned layer of NOA 81 with the embedded membrane and channel network is obtained after PDMS removal (Fig. 1, A4, B and C). PDMS stamps could be reused and only required an isopropanol/acetone wash (90/10 v/v) before a new molding. After membrane embedding, the layer retains the adhesive capability and can be stuck to a Petri dish or to a glass slide with drilled access holes. To irreversibly bind the layer to the substrate an additional UV illumination (15 s, 25 mW cm^{-2}) was applied. At this point the microdevice can be directly used for flow experiments without leaks, and solutes only permeate through the membrane (Fig. 2A). Although we focus in this article on devices made of a single layer of microfluidic channels, additional levels of microstructured resin can be stuck to the layer containing the membrane to close the device or to form a 3-D channel network.[23]

Concept and biological applications

The complete device considered later in the manuscript is composed of two parts (Fig. 2): the membrane-containing microcircuit described above, with large choice in channel network geometry, and a coverslip structured with open micro-wells, made by soft UV-lithography of NOA 81 through a mask, in which cells are plated and grown in a standard incubator (see ESI† for the complete lithography method and cell culture protocols).

Decoupling the microcircuit from cell culture micro-wells presents several significant advantages: (i) cells are grown on glass coverslips using established protocols, do not need to be maintained within a closed microenvironment for hours or days, and are easily amenable to standard cell biology techniques such as immunolabeling, transfection, RNA silencing, *etc.*; (ii) large biological samples, like explants or tissues, can be easily inserted in the device; (iii) the membrane-embedding part of the microdevice is reusable with multiple cell culture coverslips after a simple rinsing and washing procedure; and (iv) in contrast to devices where cells are directly grown on the membrane,[21,28] our systems are compatible with high N.A. oil-immersion optics, yielding optical sensitivity down to the single molecule limit.[26] Furthermore, the permeability of the membrane is not perturbed by the cell culture.

Before an experiment, cell chambers are aligned in front of membranes and the two parts are reversibly bonded using magnets (Fig. 2B). Once the device is assembled, the molecules flowing in the microchannel diffuse through the membrane and the microchamber to the targeted cells or tissues (Fig. 2D). The concentration profile applied to the cultured cells is thus determined by (i) the solute concentration profile flowing inside the microchannel above the membrane and (ii) the solute-free diffusion inside the chamber between the membrane and the cells.

Controlling the surface concentration by diffusion through the microchamber

We first quantified the temporal dependence of the diffusion process for a defined height of the microwell (200 μm). To do so, we determined the time required to reach steady-state at the coverslip surface when applying a uniform concentration profile in the microchannel (Fig. 3A and B). For three different fluorescent molecules, fluorescein, GFP and rhodamine-labeled dextran, with molecular weight ranging from 0.4 to 70 kDa, we measured the fluorescence intensity at the bottom of the microwell using total internal reflection fluorescence microscopy (TIRF-M) to avoid fluorescent background from the markers in the microchamber (Fig. 3C). We found characteristic rise times of $\tau_{FITC} \approx 35 \pm 2$ s, $\tau_{GFP} \approx 260 \pm 30$ s and $\tau_{dext70} \approx 680 \pm 88$ s, respectively.

To analyze our experimental observations, we implemented a simple two-dimensional description of the diffusion in the microchamber (Fig. 3B) and performed numerical simulations using finite element analysis (MatLab, MathWorks, MA). We considered the diffusion equation in the y, z coordinates—the x-axis corresponding to the flow direction in the microchannel—for a solute of diffusion coefficient D and concentration $c(y, z, t)$:

$$\frac{\partial c}{\partial t} = D\left(\frac{\partial^2 c}{\partial y^2} + \frac{\partial^2 c}{\partial z^2}\right) \quad (1)$$

We modeled the membrane as a semi-absorbent boundary with permeability κ, and the walls and the glass coverslip as reflective boundaries:

$$D\left.\frac{\partial c}{\partial z}\right|_{z=0^+} = \kappa\left(c(y, z=0^-, t) - c\left(y, z=0^+, t\right)\right) \quad (2)$$

$$\left.\frac{\partial c}{\partial y}\right|_{\pm w/2} = 0 \text{ and } \left.\frac{\partial c}{\partial z}\right|_{L} = 0 \quad (3)$$

The experimental results (Fig. 3C) are in agreement with the model predictions, assuming an infinite permeability κ, and

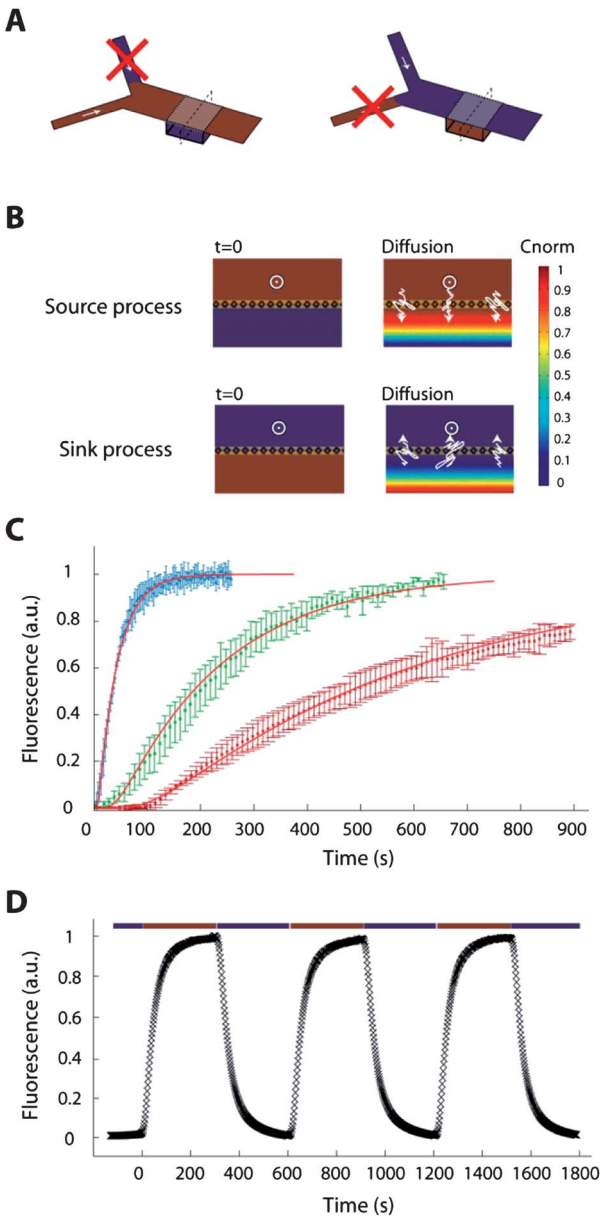

Fig. 3 Temporal characterization of the source and sink diffusive processes. (A) Scheme of a Y-shaped channel used for the measurement of the fluorescence dynamic in the microchamber. (B) Numerical simulation of the diffusive process in a transverse section of the channel and the microwell (dotted lines in A). The initial condition and the system after a short period of diffusion are represented for the source and sink processes. (C) Fluorescence intensity time course at the coverslip surface, recorded by TIRF-M, for three different markers: fluorescein (blue), GFP (green), and Dextran-70 kDa (purple). The red lines are the results of the diffusion model. (D) Fluorescence intensity time course at the coverslip for alternate flows, every 5 minutes, of FITC solution and water.

considering $D_{\mathrm{FITC}} = 450\ \mu m^2\ s^{-1}$, $D_{\mathrm{GFP}} = 92\ \mu m^2\ s^{-1}$ and $D_{\mathrm{dext70}} = 35\ \mu m^2\ s^{-1}$ as the respective diffusion coefficients of the fluorescent markers in water. The assumption of an infinite permeability coefficient κ is consistent with the fact that we are using low-binding track-etched membranes with cylindrical pores of 400 nm diameter.

With this pore size, much larger than those of the diffusible molecules, the concentration profile in the microchannel is entirely transferred to the microwell (*i.e.* $c(y, z = 0^-, t) = c(y, z = 0^+, t)$).

To further check the reversibility of the diffusion process in the microchamber, we used a Y-shaped device with manual valves at each inlet, allowing us to alternate every ~5 minutes between a uniform concentration of FITC and water. In response to this modulated stimulation, we observed oscillations of the fluorescence at the coverslip surface, confirming that the microchannel acted alternatively as a source or a sink for the fluorescent molecules in the microchamber (Fig. 3D).

Generating gradients in the membrane-based microdevice

We next used the Y-shaped circuit in a co-flow regime in order to spatially structure the concentration profiles in the microchannel. In the microchamber, an exponential gradient was generated and the profile was stable for at least 2 hours (Fig. 4A). Microchannel geometries could also be adapted to generate other simple concentration profiles. With a single-point dilution network, a two-step ladder was formed in the upper channel. For a step width inferior to twice the chamber height, this led to a linear profile at the coverslip surface (Fig. 4B). In all these cases, the profiles were also in good agreement with the results of the numerical simulations (red curves on Fig. 4), and the control of stream positions in the channel allows a spatial tuning of the gradient with good temporal resolution.

While the devices described above permit the spatially and temporally controlled generation of diffusive gradients, they impose constraints on the flow rates that can be used in the microchannels. On the one hand, a sufficiently high flow rate is required to minimize the smoothing of the concentration profile due to transverse diffusion in the upper channel; on the other hand, excessively high flow rates can generate fluxes inside the microwell, despite the membrane barrier. Considering the relative hydrodynamic resistances of the membrane and the channel, we obtain the following relation in terms of flow speed in the channel (see ESI and Fig. S1† for the derivation of eqn (4)):

$$V_{\mathrm{cells}}^{\max} \approx V_{\mathrm{c}} \frac{3\pi L^2 d_{\mathrm{pore}} r^4}{2eh_{\mathrm{microwell}} h_{\mathrm{c}}^2} \qquad (4)$$

To neglect hydrodynamic transports inside the chamber, we consider that we need a flow speed over the cells inferior to 1 $\mu m\ s^{-1}$. With e and r being the length and radius of a single pore (10 μm and 500 nm, respectively), d_{pore} the pore density, L and $h_{\mathrm{microwell}}$ the length and height of the chamber (1 mm and 50 μm, respectively) (see ESI, Fig. S1†), and h_{c} the height of the microchannel (100 μm), the flow speed is limited to ~1 $mm\ s^{-1}$. Although this condition is not particularly stringent, it places constraints on the hydraulic control—note that the size of the pores can be adapted to the flow rate required by using membranes with 100 to 200 nm pore radius.

At such a flow rate, a Y-shaped geometry remains however fluid-consuming, and the concentration profile in the channel is subjected to interface fluctuations. To overcome these limitations, we took advantage of the possibility to pattern the membrane with our microfabrication process. We developed microcircuits with two independent channels, a sink and

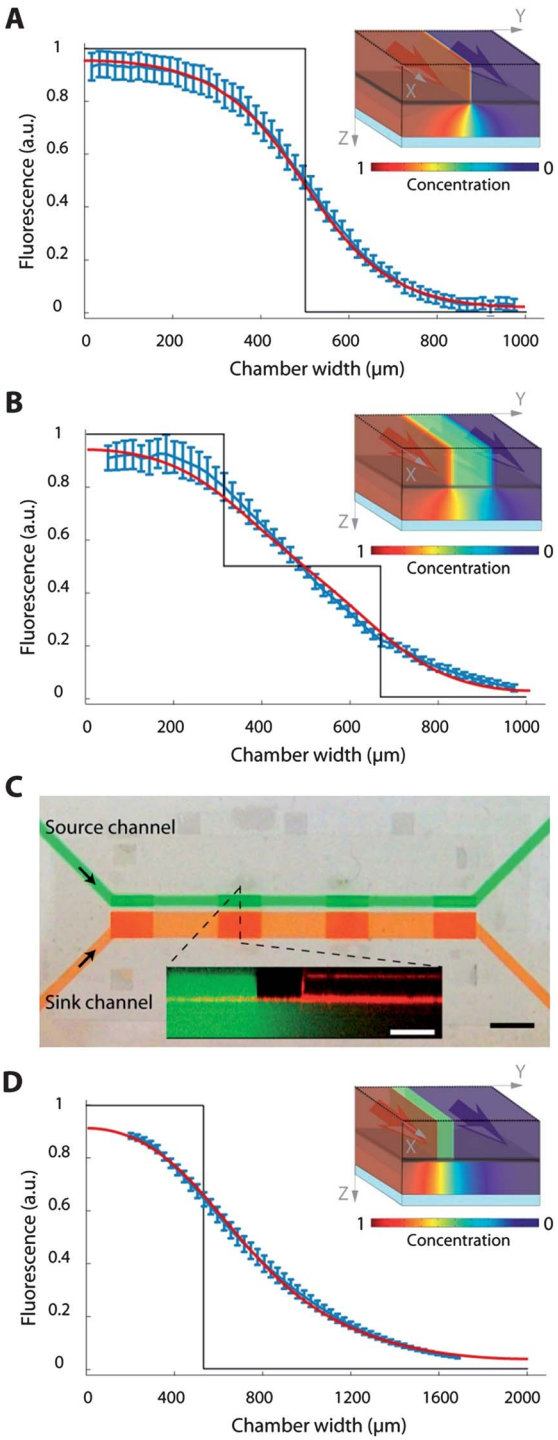

Fig. 4 Membrane based gradient generators. (A) Coflow regime in a Y shaped channel (black curve) generates a diffusive gradient in the microwell. (B) Device with a half-dilution channel (black curve) generates a linear gradient after diffusion. For A and B, confocal fluorescence measurements during 2 hours (blue curve, mean ± standard deviation) are in agreement with the numerical simulation of the concentration profile (red curve and inset). (C) Top view of a device with two independent source and sink channels. Black scale bar 2 mm. Inset: reconstruction of the transverse view by confocal imaging. White scale bar 250 μm. (D) With this geometry, a high stability diffusive gradient is obtained. Confocal measurements during 24 hours (blue curve, mean ± s.d.) are in agreement with the numerical simulation (red curve and inset).

a source, connected to the same membrane, and separated by a wall with thickness between 50 μm and 250 μm (Fig. 4C and D). The coflow geometry and the subsequent diffusive gradient are then fixed by the microfabrication and not by hydrodynamic control. Such devices, while lacking the capacity to spatially modulate the concentration profile, allow robust generation of gradients even at low flow velocity. We could obtain stable gradients over ~24 hours, with flow rates down to 5 μl min^{-1} (Fig. 4D). These devices with patterned membranes are thus particularly suited for long term experiments with biological systems that are sensitive to concentration gradients—*e.g.* during axonal pathfinding,[29] stem cell differentiation[30] or embryo development.[31]

Multiple pixel-like membrane and 2D mapping

As previously shown with the coflow device with independent channels (Fig. 4D), it is possible with our microfabrication process to pattern the membrane with multiple openings connected to independent channels. Each opening could then be differentially addressed as a source or a sink for a defined molecule and work as a single diffusive "pixel." We can thus design microdevices composed of membrane arrays which are able to dynamically generate and tune a complex concentration landscape in cell culture micro-wells.

To illustrate this possibility we present a simple three-pixel microdevice to control the rotating gradient in a round chamber.[32] The device is composed of three independent channels, each connected to a circular membrane opening of 100 μm in diameter (Fig. 5A). We attached a circular chamber (400 μm in diameter and 100 μm in height) onto the device, and alternated flows of a FITC solution and water in each channel successively using manual valves (Fig. 5B and C). By alternating the flow of solutes every 10 seconds from one channel to the next, we generated a rotating gradient of fluorescent molecules in the central region of the chamber, with an angular speed of $\omega \approx 0.2$ rad s^{-1} (see ESI, Movie M1†).

Dynamic control of complex concentration patterns by diffusive integration of flow-focused profiles

As explained above, the concentration profile at the coverslip surface results from the diffusive transfer of the profile generated in the microchannel. It is thus useful to consider the case of a "point source" in the microchannel, corresponding to an infinitely thin flow of solutes $\delta(y - y_0)$ along the y-axis and centered around y_0. Such a profile, which can be generated using a flow-focusing device, yields an elementary concentration profile $H(y,y_0)$ at the coverslip surface. Hence, an arbitrary pattern $C(y)$ in the channel leads to the concentration profile at the surface:

$$P(y) = \int H(y, y_0)C(y_0)\mathrm{d}y_0 \quad (5)$$

This simple consideration suggests an efficient way to generate a variety of complex concentration patterns at the coverslip. The principle is to sequentially recreate the profile $C(y)$ by modulating the position of the tightly focused flow in the microchannel (Fig. 6A and B) and adjusting the dwell time of the flow at each consecutive position. When the modulation is repeated with

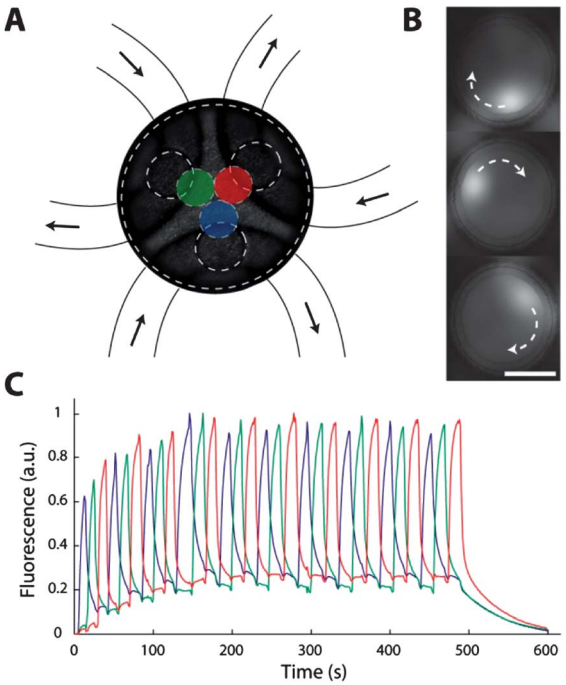

Fig. 5 Generation of concentration landscape: the rotating gradient. (A) Bright-field image of the device with 3 independent channels. The whole chamber and membrane openings are represented by dotted lines. The 3 colored areas refer to fluorescence measurement of the successive positions (see graph in C). (B) Fluorescence imaging of a FITC stream alternatively flowing in the 3 channels. Scale bar 200 μm. (C) Fluorescence intensity over time taken at three positions in the chamber (see color code in scheme A). The channel with FITC is changed every 10 seconds and the system reaches a steady state in approximately 2 minutes.

a total cycle time shorter than the diffusive transfer time through the microchamber, the profile $P(y)$ is obtained at the coverslip surface. Since the transfer time is on the order of 30 s for small molecules and focused flows can be displaced at a frequency of up to 10–20 Hz,[23] this condition is easily satisfied.

To experimentally demonstrate the method, we used a microcircuit with three independent inlets to generate a focused stream of a FITC solution (width ~100 to 250 μm) that could diffuse through the membrane in a 100 μm high microchamber (Fig. 6A).

Using electronic pressure regulators (Parker Hannifin, Precision Fluidics Division, Hollis, NH), we shifted the fluorescent stream position at a frequency of approximately 5 Hz.

An active connector[33,34] controlled by solenoid valves (The Lee Company, USA) was added at the FITC entrance of the device. This on/off fluidic connector allows for blanking the FITC "beam" with a response time of a few ms. This blanking feature is necessary to reach a low level of solute concentration between two adjacent positions of the focused "beam" of FITC. We could thus explore the whole membrane in one second, with up to five positions, to generate spatially varying concentration profiles after diffusive integration through the micro-well. The concentration of FITC at the coverslip could be varied by adjusting the residence time of the focused flow of the solute at each position along the membrane or by adding temporally controlled blanking steps at each position.

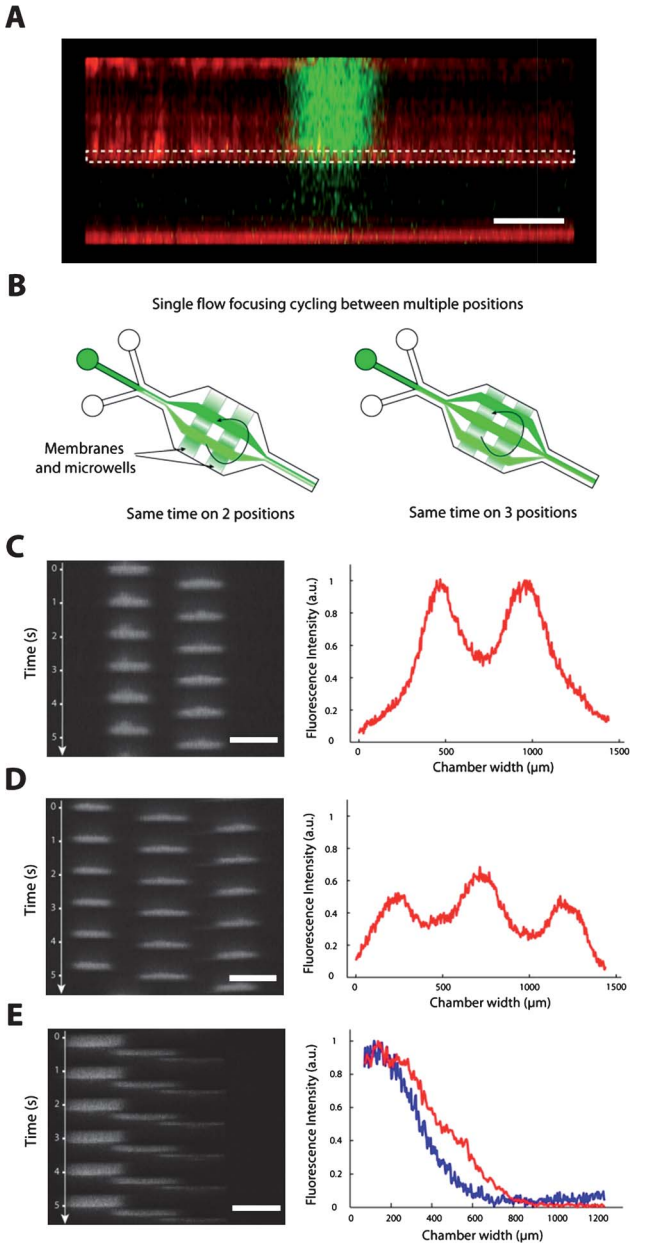

Fig. 6 Generation of complex profiles by diffusive integration of a single focused stream. (A) Reconstruction of the transverse view by confocal sectioning of a focused stream of FITC at the beginning of the diffusive process. Scale bar 100 μm. (B) Scheme of the flow focusing device cycling between 2 and 3 positions. Electronic pressure regulators and valves control the lateral extension and the timing of the stream. (C and D) Generation of various concentration profiles of FITC in the microdevices. Kymographs of the fluidic sequence in the microchannel (scale bar 250 μm) and fluorescence profiles obtained by confocal microscopy at the bottom of the microwell are represented for each condition: (C) 2 peaks, (D) 3 peaks, and (E) switch from a linear gradient (red) to a diffusive gradient (blue). The kymograph of the fluidic sequence is shown for the linear profile (scale bar 250 μm).

As a first application, we sequentially moved the single stream between 2 (or 3) positions, with equal dwell times (Fig. 6B–D). The signal in the chamber is integrated over time by diffusion, and a smoothened 2 (or 3) peak profile is observed at the bottom

coverslip. We next used the system to create gradients with a tunable slope. As shown in Fig. 6E, we could for instance generate a linear gradient by cycling between three positions with residence times of 400, 200 and 100 ms, respectively (total cycle time 850 ms) and then switch to a diffusive profile of controlled slope (*e.g.* two positions with residence times of 400 and 100 ms, respectively, kymograph not shown). With a simple flow-focusing microcircuit, it is hence possible to generate "on-demand" gradients and concentration profiles of complex shapes.

Conclusions

We present a robust method to integrate a thin nanoporous track-etched membrane within a microfluidic circuit. With this method, porous areas can be precisely defined and located on a resin layer structured with microchannels. On the opposite side of the membrane, living cells cultured on glass coverslips with pre-etched micro-wells can be positioned and a 2D chemical concentration landscape can be tailored in a shear-free environment, but dynamically controlled by tuning the fluid flows inside the microchannels. Moreover, these membrane devices based on the previously published "Microfluidic Stickers"[23,24] allow for high resolution imaging with high numerical aperture oil-immersion lens. By combining a precise and dynamic chemical concentration control, excellent imaging capabilities, a cell friendly shear-free environment and ease of use, our devices should provide unmatched performances for high-throughput cell-based assays.

Acknowledgements

We are grateful to P. Tabeling and the MMN laboratory at ESPCI for giving us access to their clean room and to B. Mathieu for his assistance on confocal imaging. We thank D. Bartolo and J.B. Salmon for useful discussions. This work was supported by grants from Fondation Pierre-Gilles de Gennes, CNRS, Fondation pour la Recherche Médicale, Centre C'Nano Ile de France and Agence Nationale pour la Recherche (ANR Piribio 2009 CONE).

Notes and references

1 N. L. Jeon, H. Baskaran, S. K. W. Dertinger, G. M. Whitesides, L. Van de Water and M. Toner, *Nat. Biotechnol.*, 2002, **20**, 826–830.
2 S. K. W. Dertinger, D. T. Chiu, N. L. Jeon and G. M. Whitesides, *Anal. Chem.*, 2001, **73**, 1240–1246.
3 S. Paliwal, P. A. Iglesias, K. Campbell, Z. Hilioti, A. Groisman and A. Levchenko, *Nature*, 2007, **446**, 46–51.
4 S. Fache, J. Dalous, M. Engelund, C. Hansen, F. Chamaraux, B. Fourcade, M. Satre, P. Devreotes and F. Bruckert, *J. Cell Sci.*, 2005, **118**, 3445–3457.
5 H. Yin, X. Zhang, N. Pattrick, N. Klauke, H. C. Cordingley, S. J. Haswell and J. M. Cooper, *Anal. Chem.*, 2007, **79**, 7139–7144.
6 K. Gupta, D.-H. Kim, D. Ellison, C. Smith, A. Kundu, J. Tuan, K.-Y. Suh and A. Levchenko, *Lab Chip*, 2010, **10**, 2019–2031.
7 C. Beta, T. Frohlich, H. U. Bodeker and E. Bodenschatz, *Lab Chip*, 2008, **8**, 1087–1096.
8 T. M. Keenan and A. Folch, *Lab Chip*, 2008, **8**, 34–57.
9 C. J. Wang, X. Li, B. Lin, S. Shim, G. L. Ming and A. Levchenko, *Lab Chip*, 2008, **8**, 227–237.
10 W. Saadi, S. W. Rhee, F. Lin, B. Vahidi, B. G. Chung and N. L. Jeon, *Biomed. Microdevices*, 2007, **9**, 627–635.
11 A. Shamloo, N. Ma, M. M. Poo, L. L. Sohn and S. C. Heilshorn, *Lab Chip*, 2008, **8**, 1292–1299.
12 S. Y. Cheng, S. Heilman, M. Wasserman, S. Archer, M. L. Shuler and M. M. Wu, *Lab Chip*, 2007, **7**, 763–769.
13 N. W. Choi, M. Cabodi, B. Held, J. P. Gleghorn, L. J. Bonassar and A. D. Stroock, *Nat. Mater.*, 2007, **6**, 908–915.
14 H. M. Yu, I. Meyvantsson, I. A. Shkel and D. J. Beebe, *Lab Chip*, 2005, **5**, 1089–1095.
15 T. M. Keenan, C. H. Hsu and A. Folch, *Appl. Phys. Lett.*, 2006, **89**, 114103.
16 N. Bhattacharjee, N. Z. Li, T. M. Keenan and A. Folch, *Integr. Biol.*, 2010, **2**, 669–679.
17 U. Haessler, M. Pisano, M. M. Wu and M. A. Swartz, *Proc. Natl. Acad. Sci. U. S. A.*, 2011, **108**, 5614–5619.
18 D. M. Cate, C. G. Sip and A. Folch, *Biomicrofluidics*, 2010, **4**, 044105.
19 G. Charvin, F. R. Cross and E. D. Siggia, *PLoS One*, 2008, **3**(1), e1468.
20 B. H. Chueh, D. Huh, C. R. Kyrtsos, T. Houssin, N. Futai and S. Takayama, *Anal. Chem.*, 2007, **79**, 3504–3508.
21 T. Kim, M. Pinelis and M. M. Maharbiz, *Biomed. Microdevices*, 2009, **11**, 65–73.
22 K. Aran, L. A. Sasso, N. Kamdar and J. D. Zahn, *Lab Chip*, 2010, **10**, 548–552.
23 D. Bartolo, G. Degre, P. Nghe and V. Studer, *Lab Chip*, 2008, **8**, 274–279.
24 M. Morel, D. Bartolo, J. C. Galas, M. Dahan and V. Studer, *Lab Chip*, 2009, **9**, 1011–1013.
25 B. G. Chung, J. W. Park, J. S. Hu, C. Huang, E. S. Monuki and N. L. Jeon, *BMC Biotechnol.*, 2007, **7**, 60.
26 M. Morel, V. Shynkar, J. C. Galas, I. Dupin, C. Bouzigues, M. Dahan and V. Studer, submitted.
27 D. C. Duffy, J. C. McDonald, O. J. A. Schueller and G. M. Whitesides, *Anal. Chem.*, 1998, **70**, 4974–4984.
28 J. J. VanDersarl, A. M. Xu and N. A. Melosh, *Lab Chip*, 2011, **11**, 3057–3063.
29 D. Mortimer, T. Fothergill, Z. Pujic, L. J. Richards and G. J. Goodhill, *Trends Neurosci.*, 2008, **31**, 90–98.
30 B. G. Chung, L. A. Flanagan, S. W. Rhee, P. H. Schwartz, A. P. Lee, E. S. Monuki and N. L. Jeon, *Lab Chip*, 2005, **5**, 401–406.
31 J. S. Kanodia, R. Rikhy, Y. Kim, V. K. Lund, R. DeLotto, J. Lippincott-Schwartz and S. Y. Shvartsman, *Proc. Natl. Acad. Sci. U. S. A.*, 2009, **106**, 21707–21712.
32 J. Atencia, J. Morrow and L. E. Locascio, *Lab Chip*, 2009, **9**, 2707–2714.
33 J. C. Galas, D. Bartolo and V. Studer, *New J. Phys.*, 2009, **11**(7), 075027.
34 M. A. Unger, H. P. Chou, T. Thorsen, A. Scherer and S. R. Quake, *Science*, 2000, **288**, 113–116.